*J. Fluid Mech.* (1975), *vol.* 72, *part* 2, *pp.* 363–371
*Printed in Great Britain*


# Axisymmetric rotating flow past a prolate spheroid

By JOHN W. MILES

Institute of Geophysics and Planetary Physics,
University of California, La Jolla

(Received 7 May 1975)

The steady, inviscid, axisymmetric, rotating flow past a prolate spheroid in an unbounded liquid is determined on the hypothesis that all streamlines originate in a uniform flow far upstream of the body. The similarity parameters for the flow are $\kappa = 2\Omega a/U$ and $\delta = a/b$, where $2a$ and $2b$ are the minor and major axes and $\Omega$ and $U$ are the angular and axial velocities of the basic flow. Solutions are obtained both by separation of variables in prolate spheroidal co-ordinates and through the slender-body limit $\delta \downarrow 0$ with $\kappa = O(1)$. Forward separation is found to occur for $\kappa > \kappa_*$, where $\kappa_*$ lies between 2·2 and 2·3 for $0 < \delta \leqslant 1$. The velocity on the body, the upstream axial velocity and the wave drag are calculated for $\kappa < \kappa_*$.

## 1. Introduction

We consider (see figure 1) a prolate spheroid in an externally unbounded, inviscid, axisymmetric, rotating flow that is (by Long's hypothesis) uniform far upstream of the body. The eccentricity of the meridional ellipse and the slenderness ratio, either of which may be chosen as the geometrical similarity parameter, are given by

$$\epsilon = b/l, \quad \delta = a/b \equiv (\epsilon^2-1)^{\frac{1}{2}}/\epsilon, \quad l = (b^2-a^2)^{\frac{1}{2}}, \qquad (1.1\,a, b, c)$$

where $2a$ and $2b$ are the minor and major axes and $2l$ is the interfocal length. The kinematical similarity parameter may be chosen as either of the inverse Rossby numbers

$$k = 2\Omega l/U, \quad \kappa = 2\Omega a/U \equiv k(\epsilon^2-1)^{\frac{1}{2}}, \qquad (1.2\,a, b)$$

where $\Omega$ and $U$ are the rotational and translational velocities of the basic flow. We seek the tangential velocity on the body, the upstream axial velocity and the wave drag as functions of $\kappa$ and $\delta$.

Both theory and experiment imply a reversed flow in the neighbourhood of the upstream stagnation point for axisymmetric rotating flow past a bluff body of revolution for sufficiently large $\kappa$, say $\kappa > \kappa_*$. The theoretical values of $\kappa_*$ for a sphere ($\delta = 1$) and a disk ($\delta = \infty$) are 2·2 and 1·9 respectively (Miles 1971, 1972). The former value is significantly larger than the value ($\kappa_* \lesssim 1$) implied by Maxworthy's (1970) observations for a sphere that is free to rotate and somewhat smaller than the value ($\kappa_* = 2{\cdot}6$) reported by Orloff & Bossel (1971) for a sphere that is constrained against rotation (the theoretical model implies that particles in the stream surface of the body have no azimuthal rotation by virtue of their origin on the upstream axis and of conservation of angular momentum along streamlines). The theoretical value for the disk is in agreement with the observed value for a disk that is constrained against rotation (Orloff & Bossel 1971).

This agreement with observation notwithstanding, the theoretical model is deficient in that it fails to account for the downstream separation that necessarily occurs in a real fluid. There are good reasons (see Miles 1971, 1972) to believe that this deficiency is of only secondary importance for the prediction of upstream flow, but it nevertheless appears desirable to carry out the corresponding calculations for a slender body (for which downstream separation is confined to a small neighbourhood of the downstream stagnation point) and to establish the dependence of upstream separation on the two parameters $\delta$ and $\kappa$ for $\delta < 1$.

Theoretical results are available (Miles 1969) in the slender-body limit $\delta \downarrow 0$ with $\kappa = O(1)$.† They appear to be adequate for the calculation of the flow far upstream of a slender ellipsoid but are not directly applicable to the calculation of stagnation-point flow. We therefore proceed to obtain a separation-of-variables solution of the boundary-value problem for any prolate spheroid ($0 < \delta \leqslant 1$) and then compare the results with those provided by a suitably modified slender-body approximation. We find that the principal results, appropriately normalized, depend primarily on $\kappa$, and are relatively insensitive to $\delta$ with $\kappa$ fixed, for $0 < \delta \leqslant 1$; in particular $\kappa_* = 2{\cdot}3$ for $\delta = 0$ and lies between $2{\cdot}3$ and $2{\cdot}2$ for $\delta \leqslant 1$. The wave drag, on the other hand, exhibits a more complicated dependence on $k$ and $\delta$.

The reader is referred to the papers cited above (especially Miles 1972) for further background and for discussion of the limitations imposed by Long's hypothesis‡ and by the appearance of closed streamlines in the downstream (lee-wave) flow for $\kappa > \kappa_c$. The available results suggest that $\kappa_c \leqslant \kappa_*$ (e.g. $\kappa_c = 1{\cdot}94$ and $\kappa_* = 2{\cdot}30$ for $\delta \downarrow 0$ and $\kappa_c = \kappa_* = 2{\cdot}2$ for $\delta = 1$), but are consistent with the hypothesis that such changes as may be induced by the closed streamlines do not significantly affect the upstream flow for $\kappa < \kappa_*$.

Frequent references will be made to Flammer's (1957) monograph on spheroidal wave functions and to Miles (1969), and equations and sections from these sources will be prefixed by F and I, respectively. The analysis closely resembles that for the oblate-spheroid solution (Miles 1972) and therefore is abbreviated. It should be noted, however, that the coefficients in the oblate-spheroidal-wave-function expansion for the circular disk are determined directly by virtue of orthogonality, whereas the determination of the corresponding coefficients for the prolate spheroid (or for an oblate spheroid of finite thickness) requires the truncation and inversion of an infinite set of linear equations.

† The slender-body limit $\delta \downarrow 0$ with $k = O(1)$ is much simpler (see Miles 1969) but is vacuous in the present context.

‡ It should perhaps be emphasized that McIntyre (1972) has demonstrated the validity of Long's hypothesis for unseparated flow with moderate $\kappa$ and $a \ll a_0$, where $a_0$ is the radius of the cylinder that actually confines the flow (radially unbounded flow is equivalent to $a/a_0 \downarrow 0$).

## 2. Boundary-value problem

After referring all lengths and velocities to $l$ and $U$, respectively, we derive the velocity from a vector potential according to

$$\mathbf{v} = \nabla \times \boldsymbol{\phi} + k\boldsymbol{\phi}, \quad \boldsymbol{\phi} = \boldsymbol{\phi}_1 \phi, \tag{2.1}$$

where $\boldsymbol{\phi}_1$ is a unit vector in the azimuthal direction of rotation, $\phi$ satisfies (Batchelor 1970, §7.5 with $\psi = Ul^2 r\phi$)

$$\phi_{xx} + \phi_{rr} + r^{-1}\phi_r + (k^2 - r^{-2})\phi = \tfrac{1}{2}k^2 r, \tag{2.2}$$

$$\phi = 0 \quad \text{on} \quad S, \quad \phi \sim \tfrac{1}{2}r + o(1/kR) \quad (kR \to \infty, x < 0), \tag{2.3a, b}$$

$R$ is the spherical radius, and $x$ and $r$ are cylindrical polar co-ordinates.

The solution of (2.2) and (2.3) for a prolate spheroid may be obtained by introducing the spheroidal co-ordinates $\xi$ and $\eta$ according to (such that $\xi = \epsilon$ on $S$)

$$x = \xi\eta, \quad r = (\xi^2 + 1)^{\frac{1}{2}}(1 - \eta^2)^{\frac{1}{2}} \quad (\xi \geqslant \epsilon, -1 \leqslant \eta \leqslant 1) \tag{2.4}$$

and expanding $\phi$ in a set of functions $\phi_n(\xi, \eta)$ that individually are $O(1/k\xi)$ in the upstream limit and are wavelike in the downstream limit [see (4.1) below]. The end result is (cf. Miles 1972, where the corresponding solution for a circular disk is developed)

$$\phi = \tfrac{1}{2}r - \tfrac{1}{2}(\epsilon^2 - 1)^{\frac{1}{2}} \sum_{n=1}^{\infty} A_n \phi_n(\xi, \eta) \tag{2.5a}$$

$$= \tfrac{1}{2} \sum_{n=1}^{\infty} [B_n\{(\xi^2 - 1)^{\frac{1}{2}} - (\epsilon^2 - 1)^{\frac{1}{2}} R_n^{(1)}(\xi)\} + (\epsilon^2 - 1)^{\frac{1}{2}} \times A_n\{R_n^{(1)}(\xi) - R_n^{(2)}(\xi)\}] S_n(\eta), \tag{2.5b}$$

where

$$R_n^{(i)}(\xi) \equiv R_{1n}^{(i)}(k, \xi)/R_{1n}^{(i)}(k, \epsilon) \quad (i = 1, 2), \tag{2.6}$$

$$S_n(\eta) \equiv S_{1n}(k, \eta) = \sum_{r=0}^{\infty} d_r^{1n} P_{r+1}^1(\eta), \tag{2.7}$$

$R_{1n}^{(1,2)}$ and $S_{1n}$ are spheroidal wave functions in the notation of Flammer (1957), $P_{r+1}^1$ is an associated Legendre function, $d_r^{1n} = 0$ for even/odd $r$ if $n$ is odd/even, the $A_n$ are determined by the boundary condition (2.3$a$) through an infinite set of simultaneous equations (the $\phi_n$ are *not* orthogonal), and

$$B_n = \frac{1}{N_{1n}} \int_{-1}^{1} (1 - \eta^2)^{\frac{1}{2}} S_n(\eta)\, d\eta = \begin{cases} 4d_0^{1n}/3N_{1n} & (n \text{ even}) \\ 0 & (n \text{ odd}), \end{cases} \tag{2.8}$$

where $N_{1n}$ is Flammer's normalizing integral for $S_{1n}$.

Turning to the meridional velocity and recalling that $v(ds/dx)$ is constant over an ellipsoid in potential flow, we introduce

$$v(\eta) \equiv v(ds/dx) = \delta(1 - \eta^2)^{-\frac{1}{2}} [\partial\phi/\partial\xi]_{\xi=\epsilon}, \tag{2.9}$$

where $ds$ is an element of meridional arc on $S$ and $\delta$ is defined by (1.1$b$). The end result implied by (2.5) and (2.9) is

$$v(\eta) = (1 - \eta^2)^{-\frac{1}{2}} \sum_{n=1}^{\infty} V_n S_n(\eta), \tag{2.10}$$

| $k$ | 1 | | 2 | | 3 | | 4 | | 5 | |
|---|---|---|---|---|---|---|---|---|---|---|
| $n$ | $A_n$ | $V_n$ | $A_n$ | $V_n$ | $A_n$ | $V_n$ | $A_n$ | $V_n$ | $A_n$ | $V_n$ |
| | | | | | $\epsilon = 1{\cdot}02$ ($\delta = 0{\cdot}197$) | | | | | |
| 1 | 1·0192 | 1·0508 | 1·0677 | 1·0448 | 1·1214 | 1·0599 | 1·1521 | 1·1005 | 1·1415 | 1·1667 |
| 2 | 0·0012 | 0·0013 | 0·0157 | 0·0170 | 0·0632 | 0·0634 | 0·1521 | 0·1420 | 0·2750 | 0·2469 |
| 3 | 0·0129 | 0·0155 | 0·0464 | 0·0545 | 0·0896 | 0·1008 | 0·1354 | 0·1429 | 0·1834 | 0·1821 |
| 4 | — | 0·0000 | 0·0002 | 0·0003 | 0·0019 | 0·0025 | 0·0092 | 0·0113 | 0·0294 | 0·0332 |
| 5 | — | 0·0001 | 0·0008 | 0·0010 | 0·0035 | 0·0047 | 0·0100 | 0·0130 | 0·0214 | 0·0265 |
| 6 | — | — | — | — | — | 0·0001 | 0·0003 | 0·0004 | 0·0015 | 0·0022 |
| 7 | — | — | — | — | — | 0·0001 | 0·0003 | 0·0005 | 0·0011 | 0·0016 |
| 8 | — | — | — | — | — | — | — | — | — | 0·0001 |
| | | | | | $\epsilon = 1{\cdot}1$ ($\delta = 0{\cdot}417$) | | | | | |
| 1 | 1·0191 | 1·0971 | 1·0552 | 1·0812 | 1·0033 | 1·2615 | 0·7270 | 1·6569 | 0·1959 | 2·3081 |
| 2 | 0·0070 | 0·0096 | 0·0806 | 0·0957 | 0·2844 | 0·2927 | 0·5824 | 0·6313 | 0·7368 | 1·2247 |
| 3 | 0·0129 | 0·0195 | 0·0469 | 0·0666 | 0·1010 | 0·1275 | 0·1991 | 0·2288 | 0·3523 | 0·4320 |
| 4 | — | 0·0001 | 0·0013 | 0·0026 | 0·0122 | 0·0217 | 0·0591 | 0·0890 | 0·2020 | 0·2548 |
| 5 | — | 0·0001 | 0·0008 | 0·0014 | 0·0037 | 0·0068 | 0·0129 | 0·0222 | 0·0431 | 0·0675 |
| 6 | — | — | — | — | 0·0003 | 0·0008 | 0·0025 | 0·0061 | 0·0137 | 0·0303 |
| 7 | — | — | — | — | 0·0001 | 0·0001 | 0·0004 | 0·0009 | 0·0019 | 0·0045 |
| 8 | — | — | — | — | — | — | 0·0001 | 0·0002 | 0·0006 | 0·0019 |
| 9 | — | — | — | — | — | — | — | — | 0·0001 | 0·0002 |
| 10 | — | — | — | — | — | — | — | — | — | 0·0001 |

TABLE 1. Representative $A_n$ and $V_n$. Blank entries imply numbers smaller than $10^{-4}$.

where $V_n$ is a linear combination of $A_n$ and $B_n$. The stagnation-point limit is given by

$$v \to \sum_{n=1}^{\infty} (-1)^{n-1} V_n c_0^{1n} \equiv v_s \quad (\eta \downarrow -1), \tag{2.11}$$

where $c_0^{1n}$ is given by F (3.2.8). Upstream separation occurs if $v_s < 0$. The limiting result for potential flow is

$$v_0 = \epsilon^{-1}[\epsilon - \tfrac{1}{2}(\epsilon^2 - 1)\log\{(\epsilon+1)/(\epsilon-1)\}]^{-1} \quad (k = 0). \tag{2.12}$$

Numerical calculations were carried out for $k = 1(1)10$ and $\xi = 1{\cdot}001$, $1{\cdot}01$, $1{\cdot}02(0{\cdot}02)1{\cdot}10$ using the tabulated $d_r^{1n}$ for $n = 1(1)10$ and $r = 0(1)21$ from Stuckey & Layton (1964) and the prolate radial functions for $n = 1(1)10$ from Hanish *et al.* (1970). Representative $A_n$ and $V_n$ are tabulated in table 1. Representative $v(\eta)$ are plotted in figure 2. The stagnation-point parameter $v_s/v_0$, which is plotted in figure 3, appears to depend primarily on the single parameter $\kappa$, and to be almost independent of $\delta$ for fixed $\kappa$, in the range $0 < \delta \leqslant 1$. (This last conclusion is supported by all of the numerical calculations, only a small part of which is plotted in figures 2–4.)

## 3. Upstream flow

The axial perturbation velocity in the direction of motion of the body relative to the fluid at rest is given by

$$u_0(\xi) = 1 - (\xi^2 - 1)^{-\frac{1}{2}}\{(1-\eta^2)^{\frac{1}{2}}\phi\}_\eta \quad (\xi \geqslant \epsilon, \quad \eta = -1). \tag{3.1}$$

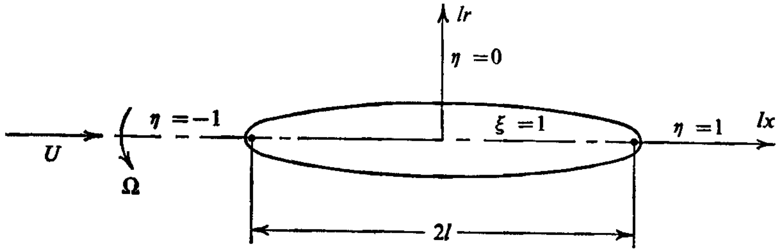


FIGURE 1. Prolate ellipsoid (meridional section) for $\epsilon = 1{\cdot}02$ ($\delta = 0{\cdot}197$).

The expansion obtained by substituting (2.5) into (3.1) converges well in the neighbourhood of the nose, where it exhibits the limiting behaviour

$$u_0 \to 1 - 2v_s\epsilon(\epsilon^2-1)^{-1}(\xi-\epsilon) \quad (\xi \downarrow \epsilon). \tag{3.2}$$

It converges only slowly for $\xi \gg \epsilon$, however, and we therefore invoke the alternative representation I (2.21 *b*):

$$u_0(-x) = \sum_{n=1}^{\infty}(-1)^{n-1}\mathscr{A}_n|x|^{-n}[1+n(n+1)(kx)^{-2}] \tag{3.3a}$$

$$\sim \mathscr{A}_1|x|^{-1} \quad (x \downarrow -\infty), \tag{3.3b}$$

where

$$\mathscr{A}_n = \tfrac{1}{2}k^2\int_{-1}^{1}\eta^{n-1}f(\eta)\,d\eta, \quad f(x) = \lim_{r\downarrow 0}(-r\phi) \tag{3.4a, b}$$

are the *upstream-influence parameters* and the dipole density of the body ($f = 0$ in $1 \leqslant |x| \leqslant \epsilon$).

The parameters $\mathscr{A}_1$ and $\mathscr{A}_2$ are plotted in figure 4. Like $v_s/v_0$ (cf. figure 3), they appear to depend primarily on the single parameter $\kappa$, and to be almost independent of $\delta$ for fixed $\kappa$, in the range $0 < \delta \leqslant 1$.

## 4. Lee-wave field

The lee-wave components of $\phi_n$ in (2.5*a*) are given by

$$\phi_n \sim 2\{R_{1n}^{(2)}(k,\epsilon)\,k\xi\}^{-1}\sin\{k\xi - \tfrac{1}{2}(n+1)\pi\}S_n(\eta) \quad (k\xi \uparrow \infty, \quad 0 < \eta \leqslant 1). \tag{4.1}$$

The corresponding wave drag on the ellipsoid, as obtained from a momentum balance over a large sphere of radius $R \uparrow \infty$, is given by [cf. I (2.25*a*) after setting $\psi \equiv \tfrac{1}{2}r^2 - r\phi$, $R \sim \xi$ and $\cos\theta \sim \eta$]

$$C_D = \{\tfrac{1}{2}\rho U^2\pi l^2(\epsilon^2-1)\}^{-1}D \tag{4.2a}$$

$$= 2\sum_{m=1}^{\infty}\sum_{n=1}^{\infty}A_mA_n[R_{1m}^{(2)}(k,\epsilon)\,R_{1n}^{(2)}(k,\epsilon)]^{-1}\cos\{\tfrac{1}{2}(m-n)\pi\}\int_0^1 S_mS_n\eta\,d\eta, \tag{4.2b}$$

where $D$ is the drag and $C_D$ is the drag coefficient.

The parametric dependence of $C_D$ on $k$ and $\delta$ appears to be less simple than that of $v_s$ and $\mathscr{A}_1$; see table 2. We observe that $C_D/k^2\delta^2$ begins to increase rapidly with $k$ for $\kappa > \kappa_c \doteqdot 2$ but that Long's hypothesis fails in this regime.

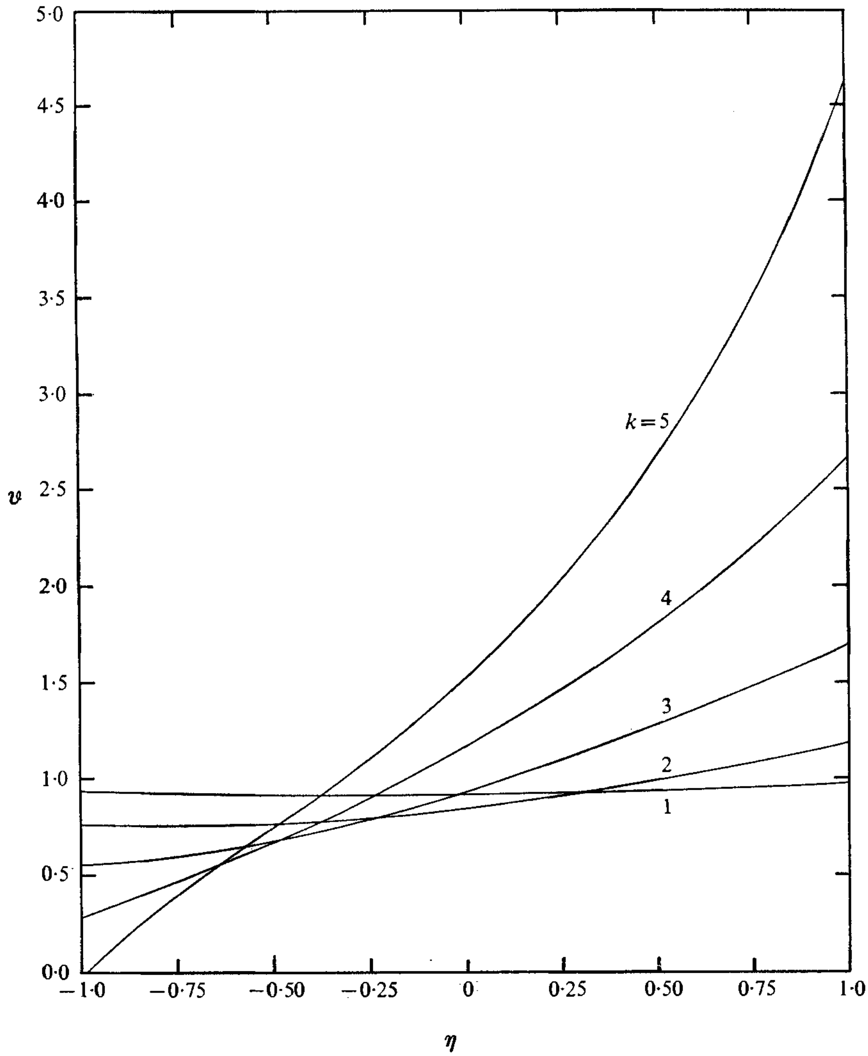


FIGURE 2. The normalized velocity distributions calculated from (2.10) for $\delta = 0{\cdot}417$ and $k = 1(1)5$.

## 5. The limit $k \uparrow \infty$, $\delta \downarrow 0$

The limit $\delta \downarrow 0$ with $\kappa = O(1)$ is considered in I §6. The results given there do not provide a uniformly valid approximation to $v$ in the neighbourhoods of $\eta = \mp 1$; however, the desired result, obtained by relating $f(\eta)$ to $v(\eta)$ [see Miles (1970, §4) regarding this relation], is

$$v_s \sim 1 - \tfrac{1}{2}\kappa^2 \exp\{-\omega_*(-1)\} \int_0^1 \{\cosh \omega_*(\eta) - \eta \sinh \omega_*(\eta)\}\{1/\Omega(\eta)\}\, d\eta \quad (k \uparrow \infty), \tag{5.1}$$

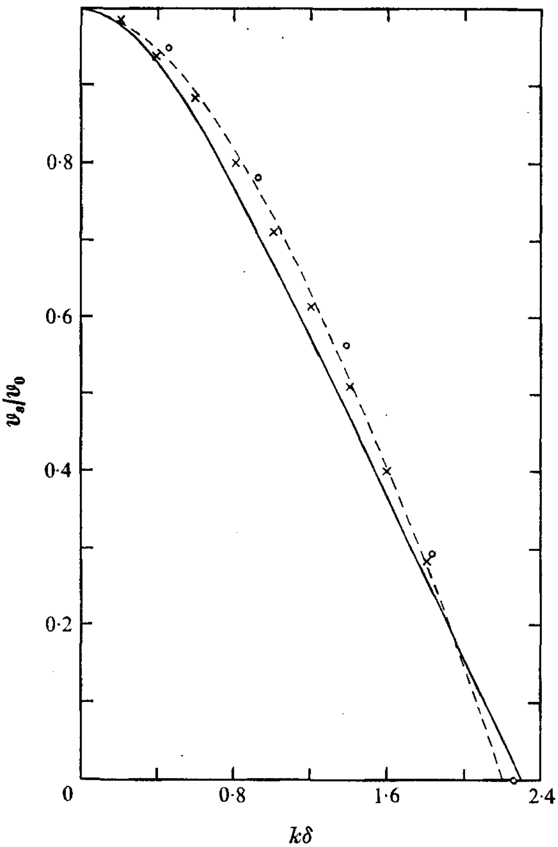


FIGURE 3. The stagnation-point parameter, calculated from (2.11) for $\delta = 0{\cdot}197$ (crosses) and $0{\cdot}417$ (circles), from (5.1) for $\delta \downarrow 0$ (solid curve) and by Miles (1971) for a sphere, $\delta = 1$ (broken curve); $v_0$, the potential-flow limit, is given by (2.12). The corresponding curve for a disk (Miles 1972), for which $\delta = \infty$, lies between those for $\delta = 0$ and $\delta = 1$ for $0 \leqslant \kappa < 1{\cdot}2$ and then drops to $v_s/v_0 = 0$ at $\kappa = 1{\cdot}9$.

where

$$\omega_*(\eta) = \tfrac{1}{2}\kappa^2 \int_0^1 \frac{\zeta}{\Omega^2(\zeta)} \log\left|\frac{\eta+\zeta}{\eta-\zeta}\right| d\zeta, \tag{5.2}$$

$$\Omega(\eta) = \tfrac{1}{2}\pi\rho\{J_1^2(\rho) + Y_1^2(\rho)\}^{\frac{1}{2}}, \quad \rho = \kappa(1-\eta^2)^{\frac{1}{2}}. \tag{5.3a, b}$$

Numerical values of $v_s$ (note that $v_0 = 1$ for $\delta = 0$) and $\mathscr{A}_1$, determined from (5.1) and I (7.10) through numerical integration, are plotted in figures 3 and 4 [the results for $\mathscr{A}_1$ do not differ significantly from those determined from the approximation I (7.14)]. Closed streamlines appear in the downstream flow for $\kappa > \kappa_c = 1{\cdot}94$ [see I (7.11)], but it seems unlikely that they significantly influence the upstream flow for $\kappa < \kappa_* = 2{\cdot}30$ (see penultimate paragraph in § 1).

This work was partially supported by the Atmospheric Sciences Section, National Science Foundation, NSF Grant DES74-23791, and by the Office of Naval Research under Contract N00014-69-A-0200-6005.

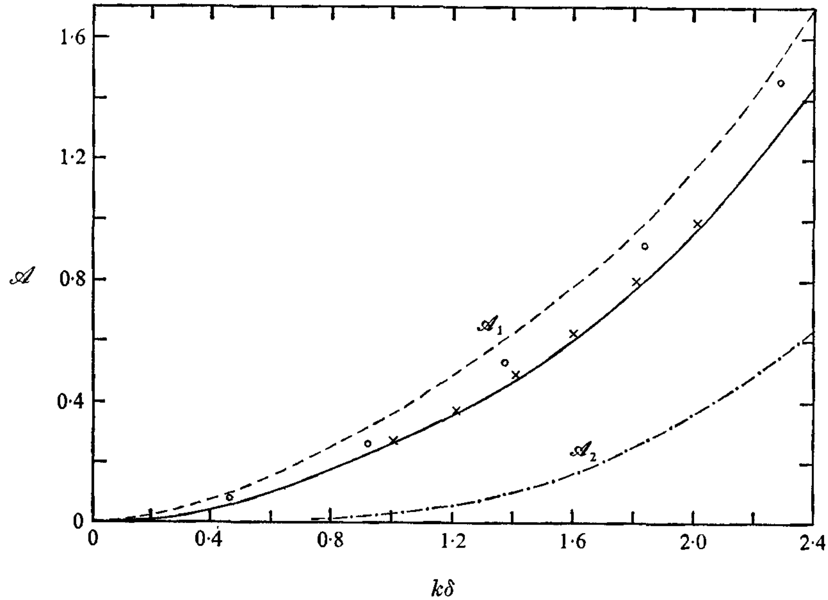


FIGURE 4. The upstream-influence parameters defined by (3.3), calculated from (2.5) and (3.4) for $\delta = 0{\cdot}197$ (crosses) and $0{\cdot}417$ (circles), from I(7.10) for $\delta \downarrow 0$ (solid curve) and by Miles (1971) for a sphere, $\delta = 1$ (broken curve). The (dot–dash) curve for $\mathscr{A}_2$ is an interpolation of the results for $0 < \delta < 0{\cdot}417$.

| | | $C_D/\kappa^2$ | | | | |
|---|---|---|---|---|---|---|
| $e$ | $\delta$ | $k = 1$ | $k = 2$ | $k = 3$ | $k = 4$ | $k = 5$ |
| 1 | 0+ | 0·208 | 0·688 | 1·160 | 1·462 | 1·627 |
| 1·001 | 0·045 | 0·210 | 0·683 | 1·125 | 1·382 | 1·486 |
| 1·02 | 0·197 | 0·226 | 0·639 | 0·901 | 0·981 | 0·989 |
| 1·04 | 0·275 | 0·239 | 0·616 | 0·822 | 0·908 | 1·011 |
| 1·06 | 0·338 | 0·250 | 0·603 | 0·793 | 0·928 | 1·169 |
| 1·08 | 0·378 | 0·260 | 0·596 | 0·790 | 1·004 | 1·449 |
| 1·1 | 0·417 | 0·268 | 0·594 | 0·808 | 1·128 | 1·875 |

TABLE 2. The modified drag coefficient $C_D/\kappa^2$ as calculated from (4.2). The entry for $k = 5$ and $e = 1{\cdot}08$ $(1{\cdot}1)$ corresponds to $\kappa = 2{\cdot}04$ $(2{\cdot}29)$, which approximates (slightly exceeds) $\kappa_c$. $C_D/\kappa^2$ increases rapidly with $\kappa$ above $\kappa_c$ (see text). The entries for $\delta = 0+$ are calculated from I (7.5).

## REFERENCES


BATCHELOR, G. K. 1970 *An Introduction to Fluid Dynamics*. Cambridge University Press.

FLAMMER, C. 1957 *Spheroidal Wave Functions*. Stanford University Press.

HANISH, S. *et al.* 1970 *Tables of Radial Spheroidal Wave Functions*, vol. 2. Washington: Naval Res. Lab., Rep. no. 7089.

MCINTYRE, M. E. 1972 On Long's hypothesis of no upstream influence in uniformly stratified or rotating flow. *J. Fluid Mech.* **52**, 209–243.

MAXWORTHY, T. 1970 The flow created by a sphere moving along the axis of a rotating, slightly viscous fluid. *J. Fluid Mech.* **40**, 453–480.

MILES, J. W. 1969 The lee-wave régime for a slender body in a rotating flow. *J. Fluid Mech.* **36**, 265–288.

MILES, J. W. 1970 The lee-wave régime for a slender body in a rotating flow. Part 2. *J. Fluid Mech.* **42**, 201–206.

MILES, J. W. 1971 Boundary-layer separation in a rotating flow. *J. Fluid Mech.* **45**, 513–526.

MILES, J. W. 1972 Axisymmetric rotating flow past a circular disk. *J. Fluid Mech.* **53**, 689–700.

ORLOFF, K. & BOSSEL, H. 1971 Laser–Doppler velocity measurements of swirling flows with upstream influence. *Bull. Am. Phys. Soc.* **16**, 1331 (abstract only).

STUCKEY, M. M. & LAYTON, L. L. 1964 *Numerical Determination of Spheroidal Wave Function Eigenvalues and Expansion Coefficients.* Washington, D.C.: David Taylor Model Basin, AML Rep. no. 164.